arXiv:cond-mat/0606335v1 [cond-mat.supr-con] 13 Jun 2006

Mixed state of a lattice d-wave superconductor

Ashot Melikyan[1,*] and Zlatko Tešanović[2,†]

[1] *Institute of Fundamental Physics, Department of Physics, University of Florida, Gainesville, FL, 32611*
[2] *Department of Physics and Astronomy, Johns Hopkins University, Baltimore, MD, 21218*

(Dated: February 2, 2022)

We study the mixed state in an extreme type-II lattice $d_{x^2-y^2}$-wave superconductor in the experimentally most relevant regime of intermediate magnetic fields $H_{c1} \ll H \ll H_{c2}$. We analyze the low energy spectrum of the problem dominated by nodal Dirac-like quasiparticles with momenta near $\mathbf{k}_F = (\pm k_D, \pm k_D)$ and find that the spectrum exhibits characteristic oscillatory behavior with respect to the product of k_D and magnetic length l. The Simon-Lee scaling, predicted in this regime, is satisfied only on average, with the magnitude of the oscillatory part of the spectrum displaying the same l^{-1} dependence as its monotonous "envelope" part. In general, the spectrum obeys a scaling law $E_{n\mathbf{k}} = \frac{\hbar v_F}{l}\mathcal{E}_n(\mathbf{k}l, t/\Delta, k_D l)$, where $\mathcal{E}$ is a dimensionless universal 2π-periodic function of $k_D l$. The oscillatory behavior of the spectrum is due to the inter-nodal interference enhanced by the singular nature of the low energy eigenfunctions near vortices. Our results constitute an example of a finite size scaling of the Dirac-type quantum criticality. We also study a separate problem of a single vortex piercing an isolated superconducting grain of size $L \times L$. Here we find that the periodicity of the quasiparticle energy oscillations with respect to $k_D L$ is doubled relative to the case where the field is zero and the vortex is absent, both such oscillatory behaviors being present at the leading order in L^{-1}. Finally, we review the overall features of the tunneling conductance experiments in YBCO and BSCCO, and suggest an interpretation of the peaks at $5-20$ meV observed in the tunneling local density of states in these materials. We find that in the case of a pure d-wave superconducting order parameter with featureless vortex cores, the zero bias conductance peak (ZBCP) appears only on the sites that are the immediate nearest neighbors of vortex locations, while all the other sites in the close vicinity of vortices exhibit no such ZBCP, and instead display pronounced peaks at sub-gap energies, typically at about a half or less of the coherence peak energy. Furthermore, we find that the on-site ZBCP can be strongly suppressed by enhanced local pairing near a vortex.

PACS numbers: 74.25.Jb, 74.25.Qt

I. INTRODUCTION

The study of the quasiparticle spectrum in the mixed state of d-wave superconductors followed soon[1,2,3] after the d-wave nature of pairing in the cuprate superconductors became apparent. A distinct character of the Tunneling Local Density of States (TLDOS) in s-wave and d-wave superconductors near a vortex was proposed by Wang and MacDonald to serve as a test which would allow determination of the pairing symmetry in the cuprates[4]. For d-wave pairing, they found that the TLDOS at the vortex location plotted as a function of energy, exhibits a prominent peak at zero applied bias voltage, while in an s-wave case, for otherwise similar parameters of the model, the thermally broadened TLDOS has a minimum at $E = 0$ surrounded by two large sub-gap peaks. While their calculations apply to densely packed vortices and unrealistically high magnetic fields in real cuprates, a similar conclusion concerning this "zero-bias peak" is obtained also within a single vortex calculation of Franz and Tešanović[5]. Interestingly, the STM experiments in BSCCO[6] and YBCO[7] – now unambiguously known to be of a d-wave type – reveal that the "zero-bias peak" is completely absent. Instead, the tunneling conductance experiences a dip at zero bias, and new relatively small sub-gap peaks at energies $5-20$ meV. To explain this discrepancy – which at the moment is unresolved – one usually relies on additional order parameters in the vortex cores. This line of thought advocates that due to the suppression of the superconducting order parameter within vortex cores, a new competing (local) order emerges there, which ultimately is responsible for the deviations from Refs. 4,5. Several different order parameters were considered in the literature: $d+id$ superconducting order[5], antiferromagnetic order[8], pseudogap state[9], circulating currents[10,11], d-density-wave[12]. Other explanations of the absent ZBCP include the anisotropy of the tunneling matrix elements[13], and, most recently, quantum zero-point motion of vortices[14].

In addition to the above "high-energy, short-distance" features of a vortex core – an interesting problem in its own right – the quest for a description of nodal quasiparticles within some simple low-energy effective Hamiltonian, which would facilitate theoretical analysis, was launched as a separate line of inquiry. An effective description is important in order to address more complicated problems such as the interactions of fluctuating vortices with nodal d-wave quasiparticles or the effects of disorder in a nodal superconductor. The initial steps in this direction were taken by Simon and Lee[15] who proposed that, after extracting the rapid "k_F" oscillations of the wavefunctions, the "linearized" effective version of the Bogoliubov-deGennes (BdG) Hamiltonian suggests a

simple scaling (15) for the low energy ($E \ll \Delta$) sector of the quasiparticle spectrum in the mixed state of type II-superconductors, and consequently for various other measurable quantities. The scaling function was then calculated by Franz and Tešanović[16], who employed a singular gauge transformation (FT transformation) and expansion of the wavefunctions in the plane wave basis to find that the spectrum at the very low energies $E \ll \hbar v_F/l$ is essentially the same as the original spectrum of the zero-field problem, but for the renormalization of the slopes of the anisotropic Dirac cones at the nodes. The linearized FT Hamiltonian was subsequently analyzed both numerically and theoretically, using its symmetry properties, in Refs. 17,18.

Further study, however, revealed several new questions. Quite separately from its origin, the linearized Hamiltonian turned out to be somewhat challenging to analyze due to singularities at vortex positions which rendered it incomplete unless its proper self-adjoint extension is constructed by imposing an additional boundary condition at each vortex[19,20]. Such boundary conditions, which turned out to be necessary in performing the numerical and symmetry analysis of the linearized Hamiltonian, are discussed at length in a companion paper[21].

Furthermore, the relation of the linearized description to the tight-binding model also turned out to be somewhat more complex than initially anticipated: the Simon-Lee scaling of the quasiparticles energy eigenstates according to (15) demands that if the spectrum is gapless on the linearized level – as found in Ref. 16 – the gaps of the full non-linearized problem must decrease as $1/l^2$ as a function of l or faster in the limit of small magnetic fields. However, exact diagonalization of the non-linearized problem at zero chemical potential $\mu = 0$, showed[19] that the gap in the spectrum oscillates between 0 and $\mathcal{O}(\hbar v_F/l)$, depending on the commensuration of the magnetic length to the atomic lattice spacing. Perhaps the most telling manifestation of the intricate relation between the linearized continuum and the tight-binding lattice models of the mixed state is the exact result[22] for the spectrum of the latter when $\mu = 0$ and $l/\delta = 2 \pmod 4$: in this case the number of the zero energy states is doubled compared to the zero magnetic field result. Clearly, such doubling is difficult to account for if one uses the non-perturbed plane wave basis as the departure point for a perturbation theory.

Here, we explore further the non-perturbative effects of the tight-binding (TB) model of a d-wave superconductor in the presence of a vortex lattice. In section II we present the results of a systematic study of the spectrum for large magnetic lengths l (low magnetic fields, corresponding to realistic values in cuprates), up to $l = 120\delta$, where δ is the lattice spacing, and for general μ. We start by focusing on the *low-energy properties of the spectrum* and analyze the validity Simon-Lee scaling for this model. The dispersion is shown to obey the scaling on *average*, and in general to experience rapid oscillations of the energy levels as a function of both the magnetic field and μ. These anomalous oscillations, which can be unified within a new generalized form of Simon-Lee scaling, are described by an additional dependence of the energy levels on the commensuration of the inter-nodal distance and magnetic length l. The inadequacy of the Simon-Lee scaling in its conventional form is shown to be the result of the singular nature of the BdG eigenfunctions combined with the inter-nodal interference, as conjectured in Refs. 19,20. The linearized effective Hamiltonian is argued to still accurately represent the low energy sector of the theory, but the necessary condition is stricter than anticipated earlier and demands also $k_F\xi \gg 1$ rather than only $k_F l \gg 1$.

In section III we describe the *high-energy, short-distance features of the spectrum*. We find that although the TLDOS is indeed peaked at the four sites of the tight-binding lattice surrounding the vortex, in agreement with previous work, the four immediate neighbors are rather an exception than a rule: all sites in the proximity of the vortex – *except* the nearest neighbors – exhibit no zero-bias peak, and furthermore have additional peaks at sub-gap energies. In the concluding section, we discuss how the on-site peak can be suppressed and argue that the $5-7$ meV peaks observed in STM experiments could in fact be due to regular d-wave vortices, but with a particular profile for the amplitude of d-wave gap function on those few bonds constituting the cores.

The anomalous enhancement of the inter-nodal interference by singular potential due to vortices has also a prominent effect on a related single vortex problem, i.e., an isolated superconducting grain of size $L \times L$ in a commensurate magnetic field $H = \Phi_0 L^{-2}$, where the elementary flux Φ_0 equals $hc/(2e)$, pierced by a single vortex. This is discussed in detail in section IV, where we show that although the spectrum has oscillations of the low energy levels of magnitude proportional L^{-1} even in zero magnetic field due to finite-size effects, in the presence of the vortex the periodicity of these oscillations is doubled.

II. TIGHT-BINDING LATTICE MODEL

A. BdG equations

We start from the Bogoliubov-deGennes(BdG) Hamiltonian H_{TB} of the model[19,20], which is defined by its action on a two-component Bogoliubov-Nambu wavefunction $\psi_{\mathbf{r}} = (u_{\mathbf{r}}, v_{\mathbf{r}})^T$ as

$$H_{TB}\psi_{\mathbf{r}} = \sum_{\mathbf{r}'} \begin{pmatrix} t_{\mathbf{r}\mathbf{r}'} - \mu\delta_{\mathbf{r}\mathbf{r}'} & \Delta_{\mathbf{r}\mathbf{r}'} \\ \Delta^*_{\mathbf{r}'\mathbf{r}} & \mu\delta_{\mathbf{r}\mathbf{r}'} - t^*_{\mathbf{r}\mathbf{r}'} \end{pmatrix} \psi_{\mathbf{r}'}. \qquad (1)$$

In the simplest case, the hopping and pairing fields described by $t_{\mathbf{r}\mathbf{r}'}$ and $\Delta_{\mathbf{r}\mathbf{r}'}$ are nonzero only on the nearest neighbor bonds, and in the presence of magnetic field $\mathbf{B}$, the hopping $t_{\mathbf{r}\mathbf{r}'} = t^*_{\mathbf{r}'\mathbf{r}}$ is modified by Peierls factors

$$t_{\mathbf{r}\mathbf{r}'} = -t\exp(-iA_{\mathbf{r}\mathbf{r}'}) \equiv -t\exp\left(-\frac{ie}{\hbar c}\int_{\mathbf{r}}^{\mathbf{r}'} \mathbf{A}\cdot d\mathbf{l}\right), \quad (2)$$

where $\mathbf{A}$ is the vector potential corresponding to magnetic field $\mathbf{B}$. The pairing field/gap function $\Delta_{\mathbf{r}\mathbf{r}'}$ should in principle be determined from a self-consistent procedure stemming from the same microscopic Hamiltonian that in the mean-field approximation yielded (1). For example, in the simplest model that results in the d-wave order within the mean-field approximation for a wide range of parameters – the extended Hubbard model with the nearest neighbors density-density attraction $gn_{\mathbf{r}}n_{\mathbf{r}'}$ – the self-consistency condition reads

$$\Delta_{\mathbf{r}\mathbf{r}'} = g\sum_n (u_{\mathbf{r}}v^*_{\mathbf{r}'} + u_{\mathbf{r}'}v^*_{\mathbf{r}}) \tanh\frac{E_n}{2T} \quad , \qquad (3)$$

where T is the temperature and (u_n, v_n) are the eigenstates of the BdG Hamiltonian of energy E_n. While incorporating the self-consistency condition is not an impossible task, the results to a certain extent will depend on the microscopic model, from which the condition was derived.

In the context of the superconductivity in cuprates, however, such dependence is very weak: the amplitude of the order parameter $|\Delta_{\mathbf{r}\mathbf{r}'}|$ recovers rapidly to its uniform state value Δ, while the phase is subject to the condition of overall winding by 2π along any lattice path enclosing a vortex. These two conditions suggest a useful simple Ansatz for the starting point of the iterative self-consistency procedure: $\Delta_{\mathbf{r}\mathbf{r}'} = \Delta\eta_{\mathbf{r}\mathbf{r}'}\exp(i\theta_{\mathbf{r}\mathbf{r}'})$, where the bond phase $\theta_{\mathbf{r}\mathbf{r}'}$ is given in the Appendix and the d-wave nature of the bond field $\Delta_{\mathbf{r}\mathbf{r}'}$ enters through factors $\eta_{\mathbf{r},\mathbf{r}+\boldsymbol{\delta}} = 1$ ($\eta_{\mathbf{r},\mathbf{r}+\boldsymbol{\delta}} = -1$) if $\boldsymbol{\delta} = \pm\delta\hat{x}$ ($\boldsymbol{\delta} = \pm\delta\hat{y}$). One then proceeds to diagonalize H_{TB} from (1), recomputes $\Delta_{\mathbf{r}\mathbf{r}'}$ using the self-consistency condition (3), and repeats the procedure until the convergence is achieved. In practice, the starting Ansatz is a very good approximation to the final solution in a sense that both have the same phase defects, the same symmetries, and the ratio of the fully self-consistent solution $\Delta_{\mathbf{r}\mathbf{r}'}$ to the Ansatz $\Delta\eta_{\mathbf{r}\mathbf{r}'}\exp(i\theta_{\mathbf{r}\mathbf{r}'})$ is merely a periodic smooth function close to unity at all bonds of the lattice, except possibly in a close proximity of vortices. Consequently, we first concentrate on the (non-selfconsistent) BdG Hamiltonian (1) with $\Delta_{\mathbf{r}\mathbf{r}'} = \Delta\eta_{\mathbf{r}\mathbf{r}'}\exp(i\theta_{\mathbf{r}\mathbf{r}'})$, which allows for an easier systematization of the results due to the reduced number of parameters and note that all possible microscopic Hamiltonians leading to d-wave pairing are now encoded by a single bond variable Δ. At the same time, this approach permits one to avoid a time-consuming search for the solution of the fully self-consistent problem. In the end, we will briefly discuss the effects of varying $\Delta_{\mathbf{r}\mathbf{r}'}$ near vortices.

$$H_{TB}\psi_{\mathbf{r}} = \sum_{\mathbf{r}'}\begin{pmatrix} -te^{-iA_{\mathbf{r}\mathbf{r}'}} & \Delta\hat{\eta}_{\mathbf{r}\mathbf{r}'}e^{i\theta_{\mathbf{r}\mathbf{r}'}} \\ \Delta\hat{\eta}_{\mathbf{r}\mathbf{r}'}e^{-i\theta_{\mathbf{r}'\mathbf{r}}} & te^{iA_{\mathbf{r}\mathbf{r}'}}\end{pmatrix}\psi_{\mathbf{r}'} - \mu\sigma_3\psi_{\mathbf{r}}, \qquad (4)$$

where the summation indices $\mathbf{r}'$ denote the nearest neighbors of $\mathbf{r}$ and σ_3 is the Pauli matrix. Although we will be interested in a periodic inversion-symmetric lattice of vortices, Hamiltonian H_{TB} does not explicitly possess the symmetries of the physical vortex lattice. In general, one has to accompany the translations by a vortex lattice vector with an additional gauge transformation restoring the Hamiltonian to its original form. Rather than working with representations of the resulting magnetic translations group, we perform a unitary transformation of a special form $U = \mathrm{diag}(e^{i\alpha_{\mathbf{r}}}, e^{-i\beta_{\mathbf{r}}})$ such that the transformed Hamiltonian $H = U^{-1}H_{TB}U$ is explicitly periodic.

It is easy to see that, regardless of the transformation used to bring the Hamiltonian H_{TB} to a periodic form, the minimal unit cell must contain at least two vortices: after the transformation the diagonal hopping term contains modified Peierls factors $\exp(i\tilde{A}_{\mathbf{r}\mathbf{r}'}) = \exp(iA_{\mathbf{r}\mathbf{r}'} + i\alpha_{\mathbf{r}'} - i\alpha_{\mathbf{r}})$. Suppose these factors are periodic, then consider a product $\prod_{\langle\mathbf{r}\mathbf{r}'\rangle} e^{i\tilde{A}_{\mathbf{r}\mathbf{r}'}}$ over the oriented bonds along a closed path formed by the perimeter of the unit cell traversed counterclockwise. Since $e^{iA_{\mathbf{r}\mathbf{r}'}} = e^{-iA_{\mathbf{r}'\mathbf{r}}}$ and factors $\exp(i\tilde{A}_{\mathbf{r}\mathbf{r}'})$ are to be periodic, such a product should be equal to 1.

$$\prod_{\langle\mathbf{r}\mathbf{r}'\rangle} e^{i\tilde{A}_{\mathbf{r}\mathbf{r}'}} = \prod_{\langle\mathbf{r}\mathbf{r}'\rangle} e^{iA_{\mathbf{r}\mathbf{r}'}} = e^{-\oint\frac{ie}{\hbar c}\mathbf{A}\cdot d\mathbf{l}} = 1.$$

Thus the flux of magnetic field through the unit cell must be an integer of $2\pi\hbar c/e = hc/e$, and therefore must contain at least two $hc/2e$ superconducting vortices.

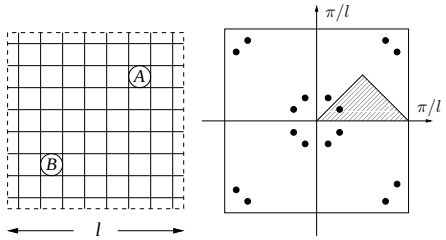


FIG. 1: Left: magnetic unit cell containing two vortices labelled as A and B with magnetic length $l = 8\delta$. Right: The symmetry of dispersion $E_{n\mathbf{k}}$ within the Brillouin zone (BZ), which follow from the symmetry operations of the Hamiltonian H, is shown. 16 equivalent points are displayed as solid dots; and it is sufficient to study only 1/16-th portion of the BZ drawn as a dashed triangle.

An explicit form of such a transformation can be realized by considering a simple family of the so-called symmetric transformations[23,24]:

$$U_{\mathbb{Z}2} = \mathrm{diag}(e^{i\alpha_{\mathbf{r}}}, e^{-i\alpha_{\mathbf{r}}}),$$

with suitably chosen $\alpha_{\mathbf{r}}$. In the continuum version of the theory this transformation forces branch-cuts and non-locality on the eigenfunctions of H'_{TB}. Although the tight-binding lattice version of it does not cause undue complications[22], here we utilize another common

choice, the FT transformation[16], whose continuum analogue does not require branch-cuts:

$$U = \mathrm{diag}(e^{i\phi^A_{\mathbf{r}}}, e^{-i\phi^B_{\mathbf{r}}}), \tag{5}$$

where site variables ϕ_A and ϕ_B are explicitly given in the Appendix A of Ref. 21. After defining periodic[19,21] bond variables $\mathcal{V}^A_{\mathbf{rr}'}$, $\mathcal{V}^B_{\mathbf{rr}'}$, and $\mathcal{A}_{\mathbf{rr}'}$ according to

$$\mathcal{V}^{A(B)}_{\mathbf{rr}'} = \phi^{A(B)}_{\mathbf{r}'} - \phi^{A(B)}_{\mathbf{r}} - A_{\mathbf{rr}'} \tag{6}$$

$$\mathcal{A}_{\mathbf{rr}'} = \theta_{\mathbf{rr}'} - \phi^A_{\mathbf{r}} - \phi^B_{\mathbf{r}'}, \tag{7}$$

the resulting periodic Hamiltonian is given by

$$H\psi_{\mathbf{r}} = \sum_{\mathbf{r}'} \begin{pmatrix} -te^{i\mathcal{V}^A_{\mathbf{rr}'}} & \Delta\hat{\eta}_{\mathbf{rr}'}e^{i\mathcal{A}_{\mathbf{rr}'}} \\ \Delta\hat{\eta}_{\mathbf{rr}'}e^{-i\mathcal{A}_{\mathbf{r}'\mathbf{r}}}u_{\mathbf{r}'} & te^{-i\mathcal{V}^B_{\mathbf{rr}'}} \end{pmatrix} \psi_{\mathbf{r}'} - \mu\sigma_3\psi_{\mathbf{r}} \tag{8}$$

with $\mathbf{r}'$ denoting the nearest neighbors of $\mathbf{r}$.

B. Linearization of the tight-binding Hamiltonian

One can now attempt to describe the low energy portion of the quasiparticle spectrum using the linearized approximation, leading to Simon-Lee scaling for various properties. The derivation of the linearized version of H_{TB} has been performed in Refs. 19,20 by gradient expansion resulting in a continuum Hamiltonian with dispersion, which is then linearized as usual[16]. One might expect that the coefficients of the final model obtained in this way reproduce the spectrum of the full TB model for the values of chemical potential μ not too close to the half-filling – where the dispersion is not quadratic – and also for μ not too close to the bottom of the tight-binding band, otherwise the linearization procedure itself is not justified. Below, we describe an alternative derivation which, while proceeding along similar lines as the standard procedure, does lift the first restriction and allows one to consider values of μ at and near half-filling. At the end of this section, we will revisit this derivation and show that it should be corrected to accommodate the curvature and the so-called "interference" effects.

The linearization procedure is based on the assumption that wavefunctions can be represented as

$$\psi_{\mathbf{r}} = \sum_{j=1,\overline{1},2,\overline{2}} e^{i\mathbf{k}^{(j)}_F\cdot\mathbf{r}}\psi^{(j)}(\mathbf{r}) \quad , \tag{9}$$

where j labels the Dirac-like nodes of a d-wave gap function located in momentum space at $\mathbf{k}^{(j)}_F = (\pm k_D, \pm k_D)$, and $\psi^{(j)}(\mathbf{r})$ is slowly varying function on the scale of k_F^{-1}. Variable k_D introduced here for brevity of notation simply equals $k_F/\sqrt{2}$, where k_F is the magnitude of the Fermi momentum in a nodal direction. After substituting this form into the BdG eigenvalue problem for Hamiltonian H (8), a typical term has the form of a sum over $\boldsymbol{\delta} = \pm\delta\hat{x}, \pm\delta\hat{y}$:

$$S = \sum_{\boldsymbol{\delta}} e^{i\int_{\mathbf{r}}^{\mathbf{r}+\boldsymbol{\delta}}\mathbf{w}\cdot d\mathbf{l}} f_{\mathbf{r}+\boldsymbol{\delta}} \quad , \tag{10}$$

where Fourier transform of $f_{\mathbf{r}}$ is assumed to be composed of wavevectors close to the four nodal momenta at the Fermi surface and $\nabla\cdot\mathbf{w} = 0$. Note that the straightforward gradient expansion is valid only qualitatively since $k_F\delta$ is not necessarily much smaller than one. The linearization, however, can be performed directly, without the preliminary "continuization" step, by first separating the rapidly oscillating part:

$$f_{\mathbf{r}} = e^{i\mathbf{k}^{(j)}_F\cdot\mathbf{r}}F_{\mathbf{r}} \quad ,$$

where $F_{\mathbf{r}}$ is a function that changes slowly on the scale of few lattice spacings. To obtain the effective linearized description, we now replace the lattice function $F_{\mathbf{r}}$ by a slowly changing function $F(\mathbf{r})$ defined in continuum, such that it coincides with $F_{\mathbf{r}}$ when $\mathbf{r}$ correspond to the lattice sites. Thus, $F(\mathbf{r})$ can be thought of as an interpolating function for a discrete set $F_{\mathbf{r}}$. The detailed form of the interpolation turns out unimportant for the leading order results derived below, as long as the characteristic scale on which $F_{\mathbf{r}}$ varies is much larger than the lattice spacing δ. Then, in the expression

$$S = e^{i\mathbf{k}^{(j)}_F\cdot\mathbf{r}}\sum_{\boldsymbol{\delta}} e^{i\int_{\mathbf{r}}^{\mathbf{r}+\boldsymbol{\delta}}\mathbf{w}\cdot d\mathbf{l}}e^{i\mathbf{k}^{(j)}_F\cdot\boldsymbol{\delta}}F(\mathbf{r}+\boldsymbol{\delta}) \quad ,$$

we use

$$e^{i\int_{\mathbf{r}}^{\mathbf{r}\pm\delta\hat{x}}\mathbf{w}\cdot d\mathbf{l}} = 1 \pm iw_x\delta - \frac{w_x^2\delta^2}{2} + \frac{i\delta^2}{2}\nabla_x w_x \quad .$$

and expand slowly varying function $F(\mathbf{r})$ into Taylor series while retaining factors $\exp(i\mathbf{k}^{(j)}_F\cdot\boldsymbol{\delta})$. The result for node $\mathbf{k}^{(1)}_F = (k_D, k_D)$ is

$$S = -e^{i\mathbf{k}^{(1)}_F\mathbf{r}}\left[2\sqrt{2}\delta\sin(k_D\delta)\left(\frac{p_x+p_y}{\sqrt{2}} + \frac{w_x+w_y}{\sqrt{2}}\right)F + \delta^2\cos(k_D\delta)(\mathbf{p}+\mathbf{w})^2F + \ldots\right], \tag{11}$$

where $\mathbf{p}$ denotes the usual continuum momentum operator $-i\nabla$, and $\ldots$ denote terms containing higher powers of $\delta\nabla$ and $\delta\mathbf{w}$.

The expressions for the off-diagonal terms of (8) differ only by the presence of the factor $\eta_{\boldsymbol{\delta}}$:

$$S' = \sum_{\boldsymbol{\delta}} \eta_{\boldsymbol{\delta}} e^{i\int_{\mathbf{r}}^{\mathbf{r}+\boldsymbol{\delta}}\mathbf{w}\cdot d\mathbf{l}} f_{\mathbf{r}+\boldsymbol{\delta}} \quad ,$$

and after similar algebra we find

$$S' = e^{i\mathbf{k}^{(1)}_F\mathbf{r}}\Big[2\sqrt{2}\delta\sin(k_D\delta)\left(\frac{p_y-p_x}{\sqrt{2}} + \frac{w_y-w_x}{\sqrt{2}}\right)F - \delta^2\cos(k_D\delta)((p_x+w_x)^2 - (p_y+w_y)^2)F + \ldots\Big], \tag{12}$$

Using the expressions for S and S', in the leading order we obtain

$$H_{lin} = v_F\frac{\Pi_x+\Pi_y}{\sqrt{2}}\sigma_3 + v_\Delta\frac{\Pi_y-\Pi_x}{\sqrt{2}}\sigma_1 + v_F\frac{v_x+v_y}{\sqrt{2}} \tag{13}$$

where the effective velocities v_F and v_Δ are given by the zero-field expressions given in the next subsection (18), $\mathbf{v}$ is the superfluid velocity, and $\Pi_i = p_i + a_i$ is the generalized momentum with $\mathbf{a} = (\mathbf{v}_A - \mathbf{v}_B)/2$ describing the vector potential due to an array of Aharonov-Bohm π-fluxes located at vortices of subset A and similarly $-\pi$-fluxes at vortices of subset B. Since the only length in this effective low-energy Hamiltonian (13) is the magnetic length l, it immediately follows

$$H_{lin}(\mathbf{r}, l, v_F, v_\Delta) = \frac{\hbar v_F}{l} H_{lin}(\mathbf{r}/l, v_F/v_\Delta), \qquad (14)$$

and, consequently, the spectrum of this Hamiltonian must satisfy the Simon-Lee scaling relation for the low energy eigenstates:

$$E_n(\mathbf{k}) = \frac{\hbar v_F}{l} E_n^*(\mathbf{k}l, v_F/v_\Delta) \quad . \qquad (15)$$

C. Zero field spectrum

Let us briefly summarize the properties of the spectrum in the absence of a magnetic field, which is obtained from (8) by setting the field-induced factors $\exp(i\mathcal{A}_{\mathbf{rr}'})$ and $\exp(i\mathcal{V}^{A(B)}_{\mathbf{rr}'})$ to zero. The excitation spectrum in this case is

$$\epsilon_{\mathbf{k}} = \pm\sqrt{\xi^2_{\mathbf{k}} + \Delta^2_{\mathbf{k}}}, \quad -\pi/\delta \le k_{x,y} < \pi/\delta$$

where $\xi_{\mathbf{k}} = -2t(\cos k_x\delta + \cos k_y\delta) - \mu$ and the d-wave pairing gap function is $\Delta_{\mathbf{k}} = 2\Delta(\cos k_x\delta - \cos k_y\delta)$. The four nodal points ($i = 1, \ldots, 4$) of the spectrum are located at $\mathbf{k}_F^{(j)} = (\pm k_D, \pm k_D)$, where

$$k_D = \frac{1}{\delta}\arccos\left(-\frac{\mu}{4t}\right). \qquad (16)$$

All four nodes merge at $\mu = \pm 4t$, while at $\mu = 0$ the inter-nodal separation is the largest. The dispersion in the vicinity of each node can be approximated as $\epsilon_{\mathbf{k}} = \sqrt{v_F^2\delta k_\perp^2 + v_\Delta^2\delta k_\parallel^2}$, where $\delta k_\perp (\delta k_\parallel)$ is the displacement of the momentum from a nodal point in the direction perpendicular (parallel) to the Fermi surface, and the effective velocities are

$$v_F = 2\sqrt{2}a\sqrt{1 - \left(\frac{\mu}{4t}\right)^2}\, t \qquad (17)$$

$$v_\Delta = 2\sqrt{2}a\sqrt{1 - \left(\frac{\mu}{4t}\right)^2}\,\Delta \quad . \qquad (18)$$

D. Spectrum in a magnetic field: $\mu = 0$ (known results)

The structure of the spectrum in a finite magnetic field is a great deal more complex. In all cases, the spectrum at energies much larger than Δ evolves to a set of sharp – conventional Schrödinger, as opposed to Dirac – Landau levels, while at low energies is characterized by strongly dispersive energy bands. For concreteness, we will consider a square lattice of vortices oriented as shown in Fig. 1 with a unit cell of minimal area, which contains two vortices, labelled A and B. In addition, we will only study the values of magnetic field that correspond to the symmetric placement of vortices within plaquettes – this requirement restricts the values of magnetic length l to even integers in the units of lattice spacing.

Let us first recall the results for a fully particle-hole symmetric system[19,20,22], corresponding to $\mu = 0$. Due to a special symmetry ($\psi_{\mathbf{r}} \to (-1)^{(x+y)/\delta}\psi_{\mathbf{r}}$) of this case, the spectrum is doubly degenerate for all momenta $\mathbf{k}$. As shown in Ref. 22, when the center of inversion for the vortex lattice coincides with a site of the atomic lattice – a situation realized for magnetic lengths $l/\delta \equiv 2 \pmod 4$– the spectrum contains *eight* Dirac nodes (*sixteen* zero energy states): two degenerate nodes at each of the four momenta $\mathbf{k} = (\pm\frac{\pi}{2l}, \pm\frac{\pi}{2l})$. This is quite unusual non-perturbative result, since it suggests that for arbitrarily small fields giving rise to a vortex lattice, the number of zero modes is doubled compared to the four nodes of the zero-field problem, provided the magnetic length has the correct commensuration with the tight-binding lattice spacing.

In the opposite case $l/\delta \equiv 0 \pmod 4$, the symmetry does not demand the zero modes, and, as was found numerically in Ref. 19, the field-induced gap in this case scales as l^{-1} as a function of magnetic length within the regime $H_{c1} \ll H \ll H_{c2}$. This result is also surprising, since for the lowest energies, one expects to recover the Simon-Lee scaling of the linearized problem (15).

The existence of the nodes for commensuration $l/\delta \equiv 2 \pmod 4$ might suggest that the spectrum of the linearized problem given by E^* in (15) is gapless – this is also a result obtained earlier[16,17] from the analysis of the linearized Hamiltonian. This conclusion in turn would have required that in the expansion of the overall field-induced gap

$$\Delta_m = \alpha_1\frac{1}{l} + \alpha_1\frac{1}{l^2} + \ldots$$

the leading $1/l$ term is absent, and only small gaps of order $1/l^2$ should generally appear from the terms that were left out in the process of linearization.

The large gaps whose size scales as $1/l$ for weak magnetic fields in a particle-hole symmetric situations at commensuration factors $l/\delta \equiv 0 \pmod 4$, as was found in Refs. 19,20, therefore come entirely unexpected. These large gaps were interpreted as as the effect of the inter-nodal interference, and such effects for the deliberately distorted lattice were indeed found to be suppressed. It was argued that in realistic situations a weak disorder in vortex positions or the one due to impurities will suppresses these interference effects. Yet, the following questions remain to be answered: First, is this

situation specific only to a particle-hole symmetric system ($\mu = 0$)? Second, how could the scaling relation (15) be explicitly violated, even for an ideal periodic lattice? Finally, how – if at all – the Simon-Lee scaling can be recovered in the tight-binding problem without introducing the disorder explicitly?

E. The spectrum for general μ

We start by answering the first of these question and consider the spectrum for non-particle-hole symmetric systems ($\mu \neq 0$). We show below that the rather involved behavior displayed by the spectrum as a function of μ and l in fact follows a simple universal pattern when expressed in terms of suitably rescaled variables. For the square lattice of vortices considered here, the analysis is further simplified due to the sixteen-fold symmetry of the dispersion $E_{n\mathbf{k}}$ within the Brillouin zone illustrated in Fig. 1. Furthermore, using a transformation $\psi_{\mathbf{r}} \to (-1)^{(x+y)/\delta}\psi_{\mathbf{r}}$ and the symmetry of the spectrum at each $\mathbf{k}$ as a function of energy (see Appendix), it is easy to show that the spectra at values of chemical potential $+\mu$ and $-\mu$ are identical, with or without magnetic field, and therefore in what follows we assume $\mu > 0$.

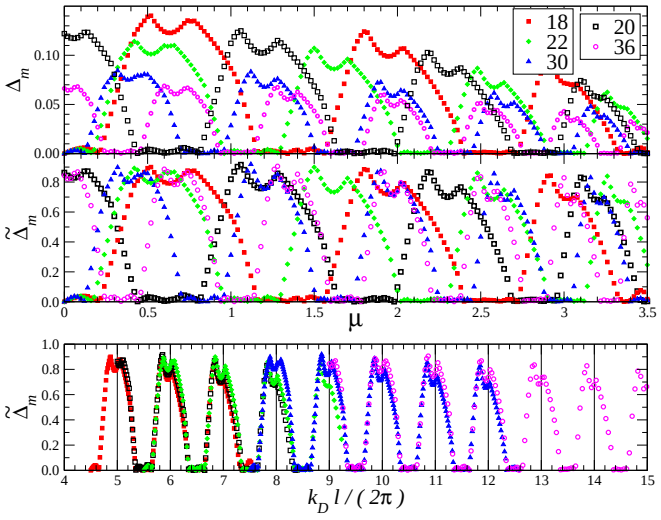


FIG. 2: Upper panel: The overall gap Δ_m induced by vortex lattice as a function of chemical potential μ. The parameters are $\Delta = t$, $l/\delta = 18, 22, 30$ (solid symbols) and $l = 36\delta$ (open symbols). Center panel: the gaps are renormalized by l/v_F according to the Simon-Lee prescription: $\tilde{\Delta}_m = \Delta_m l/\hbar v_F$. In the limit of small magnetic field the result should have been independent of μ in direct contradiction with explicit numerical evaluation shown here. Lower panel: instead of the chemical potential μ, the horizontal axis represents $k_D l/(2\pi)$. In the limit of low magnetic fields ($l \gg \delta$) all curves representing dependence of $\tilde{\Delta}_m$ on lk_D collapse onto a 2π-periodic function. For fixed l, deviations from this universal scaling are the largest for μ close to the bottom of the tight-binding band, where the Fermi surface is small and the validity condition for linearization ($lk_F \gg 2\pi$) is violated.

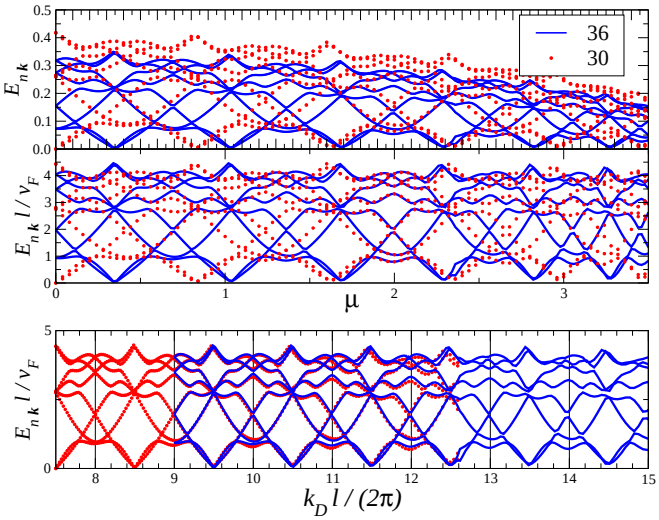


FIG. 3: Upper panel: The dependence of the lowest eight positive energy bands $E_{n\mathbf{k}}$ at fixed momentum $\mathbf{k}_0 l = (\pi/2, \pi/2)$ on chemical potential μ. The parameters are $\Delta = t$, $l/\delta = 30, 36$. Note that the two values of magnetic length l correspond to the gapped ($l/\delta = 4n$) and gapless ($l/\delta = 4n + 2$) families at half-filling ($\mu = 0$). Center panel: the energy levels at $\mathbf{k}_0$ are rescaled by l/v_F. Lower panel: Instead of the chemical potential μ, the horizontal axis represents $lk_D/(2\pi)$. In the limit of low magnetic fields ($l \gg \delta$) all curves representing dependence of $\tilde{\Delta}_m$ on $k_D l$ collapse onto a 2π-periodic function.

The field-induced gap for $v_F = v_\Delta$ is plotted as a function of the chemical potential μ in the upper panel of Fig. 2 for several values of magnetic length l. At all magnetic fields the dependence on μ displays a characteristic oscillatory behavior. For the family of magnetic lengths $l = (4n + 2)\delta$, the spectrum is gapless at $\mu = 0$, in accordance with the previous results[19], and for a finite fraction of one cycle of oscillations in μ the field-induced gaps are extremely small, their size quite possibly set by l^{-2} in the scaling limit: we were not able to definitely establish the scaling behavior due to the smallness of the gaps in this regime. Then the gaps increase and remain large – of order $\hbar v_F/l$ – for about a third of the cycle, until eventually again turning to zero. This cycle is then repeated over and over. For $l = 4n\delta$ the only difference is that the cycle is offset by half a period in μ. The overall slow decrease of the average gap size for large values of μ follows directly from the Simon-Lee scaling (15) as v_F decreases with μ (see Eq. (18)). To account for the expected Simon-Lee scaling, the central panel of Fig. 2 shows the rescaled gap

$$\tilde{\Delta}_m = \frac{\Delta_m l}{\hbar v_F}$$

as a function of μ. If Simon-Lee scaling in its original form were exact, one would expect to see no dependence μ. Instead, for any given field value, the rescaled gap $\tilde{\Delta}_m$ itself exhibits oscillatory behavior.

Still, comparing the upper panel of Fig. 2 one must conclude that $\tilde{\Delta}_m$ is a step forward compared to Δ_m; *on*

average the curves representing different magnetic field and different values of μ look almost identical. Although the detailed analytic theory of the "interference effects" remains a challenge for the future, the essence of such interference is vividly illustrated by replotting the family of $\tilde{\Delta}_m$ as function of $lk_D/(2\pi)$. So rescaled, all curves collapse into a single universal periodic function shown in the third panel of Fig. 2.

We find that the above oscillatory behavior is not specific to the field-induced gap function; the dependence of the entire spectrum $E_n(l\mathbf{k})$ is characterized by similar behavior. As an example, Fig. 3 displays the eight lowest energy levels at $\mathbf{k} = (0, 0)$ for $l = 30\delta$ and $l = 36\delta$, representing two families of magnetic fields. The central panel shows the energy levels rescaled by v_F/l, while the bottom panel shows that the remaining oscillations of the rescaled spectrum fall onto a universal periodic curve if plotted as functions of $k_D l$ rather than μ.

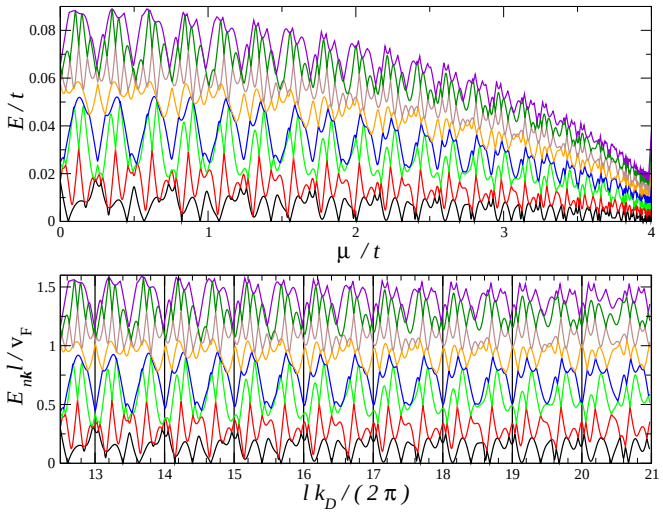


FIG. 4: Upper panel: The dependence of the lowest eight positive energy bands $E_{n\mathbf{k}}$ at fixed momentum $\mathbf{k}_0 l = (0, 0)$ on chemical potential μ. The parameters are $\Delta = 0.2t$, $l = 50\delta$. Lower panel: Instead of the chemical potential μ, the horizontal axis represents $lk_D/(2\pi)$. Only the range $0 < \mu < 3.5t$ is plotted in the lower panel.

The pattern just described is not restricted to the isotropic case $\alpha_\Delta = v_F/v_\Delta = 1$ and holds for all α_Δ we checked (2, 5, 10, 20, 50). For large anisotropies, the deviations from the scaling behavior become more pronounced at smaller values of l due to violation of the $\hbar\omega_c \ll \Delta$ condition, which translates to $l/\delta \gg \sqrt{\alpha_\Delta}$ – this condition is necessary if we are to treat magnetic field as a "small" perturbation of a zero-field d-wave superconductor. Fig. 4 illustrates the spectrum at $k = 0$ for the anisotropic case $\alpha_\Delta = 5$. In all cases, for sufficiently weak magnetic fields, the spectrum still exhibits 2π-periodic oscillations in $k_D l$ of amplitude $C\hbar v_F/l$, where the numerical prefactor C is only a function of t/Δ. We stress that the oscillatory part of the spectrum is of the same order of magnitude as its smooth, "envelope" dependence, and is not smaller than this average Simon-Lee envelope part in any sense. These results can be summarized in the following scaling form:

$$E_{n\mathbf{k}} = \frac{\hbar v_F}{l}\mathcal{E}_n(\mathbf{k}l, t/\Delta, k_D l), \tag{19}$$

where $\mathcal{E}$ is a universal dimensionless function, which is 2π-periodic with respect to its last argument. This scaling, which combines the oscillations with respect to both magnetic field and the chemical potential, holds for all values of chemical potential, except when μ is very close to the bottom of the band – in this case the scaling was studied by Vafek and Tešanović[25].

The origin of this oscillatory behavior can be traced back to the linearization procedure. Recall that the matrix elements of the FT-transformed, but yet nonlinearized Hamiltonian $\mathcal{H}$ (8) are evaluated in the plane wave basis. By inspection, in the limit $lk_D \gg 1$, the leading term of this infinite matrix $\mathcal{H}_{\mathbf{k}\mathbf{k}'}$ appears to have a block-diagonal form, with each of the four blocks corresponding to separate nodes. Within each block, only the leading order approximation in l^{-1} is kept, while the block-offdiagonal (inter-nodal) matrix elements as well as the higher-order corrections to the block-diagonal (intra-nodal) matrix elements, which superficially scale at worst as l^{-2} , are neglected. Therefore, by construction, the matrix elements of each block precisely coincide with the matrix elements of the linearized Hamiltonian. What we found, however[20,21], is that the situation is not this simple: this description is necessarily incomplete due to the singular character of the linearized problem wavefunctions near vortices. Consequently, the linearized Hamiltonian requires self-adjoint extensions, obtained by imposing additional boundary conditions near vortices, which themselves are ultimately determined by those "higher-order terms" which were dropped in the oversimplified analysis.

A straightforward way to appreciate the significance of these subdominant terms is actually to recompute the matrix elements of the full Hamiltonian – not in the plane-wave basis as one naturally would within a pedestrian perturbation theory – but with respect to the exact eigenfunctions of the linearized problem[26] with fixed boundary conditions at vortex locations $\{\theta\}$. The wavefunctions of the linearized Hamiltonian diverge near vortices[21] as $r^{-1/2}$, and therefore the eigenfunctions of the linearized Hamiltonian at each node can be written as

$$\Psi^{(j)}_{\mathbf{k},n}(\mathbf{r}) = e^{i\mathbf{k}^{(j)}_F\cdot\mathbf{r}}\left(\frac{1}{\sqrt{l|\mathbf{r}-\mathbf{R}_A|}}\chi^{(jA)}_{\mathbf{k},n}(\mathbf{r}/l) + \frac{1}{\sqrt{l|\mathbf{r}-\mathbf{R}_B|}}\chi^{(jB)}_{\mathbf{k},n}(\mathbf{r}/l) + \frac{1}{l}f_{\mathbf{k},n}(\mathbf{r}/l)\right), \tag{20}$$

where i labels the nodes $1, \overline{1}, 2$, and $\overline{2}$, $\mathbf{k}$ is the Bloch momentum, n is the band index, and dimensionless continuous functions χ and f are such that the expression in the

brackets is Bloch-periodic. Note that if the wavefunctions contained only the regular part, the terms retained in the linearized Hamiltonian would be of the order $\hbar v_F/l$, while the non-linear terms such as $m\mathbf{v}^2_{A(B)}/2$, $\mathbf{a}^2$ etc, would contain *an additional* factor of $(k_F l)^{-1}\ln(l/\xi)$, and could have been safely omitted. The presence of the divergent part of the wavefunctions described by the first part of (20), however, changes the situation. Let us evaluate again the structure of the matrix elements $\langle\Psi^{(j')}_{n\mathbf{k}}|\mathcal{H}|\Psi^{(j)}_{n'\mathbf{k}'}\rangle$ between the states at momenta $\mathbf{k}$ and $\mathbf{k}'$ differing by reciprocal lattice vector $\mathbf{G}$. The intra-nodal matrix elements with $j = j'$ to the leading order are just the eigenstates of the linearized Hamiltonian $\hbar v_F E^*_n(\mathbf{k}l)\delta_{nn'}/l$. The corrections due to non-linear terms, however, quite peculiarly also exhibit the same scaling as a function of magnetic length l as we will argue now. Consider a typical non-linear term $m\mathbf{v}^2/2$, since $(m\mathbf{v})^2$ increases near vortices as $1/r^2$ down to distances of the core size $\sim\xi$, to the leading order the matrix element

$$\left\langle \Psi^{(j)}_{n\mathbf{k}}\middle|\frac{m\mathbf{v}^2}{2}\middle|\Psi^{(j)}_{n'\mathbf{k}'}\right\rangle \propto \int_\xi^l (rl)^{-1/2}\frac{r^{-2}}{m}(rl)^{-1/2}(rdr) \propto \frac{v_F}{l}\frac{1}{k_F\xi} \quad (21)$$

has the $1/l$ scaling. Higher-order curvature terms containing higher order derivative operators and potentials $\mathbf{a}$ or $\mathbf{v}$ can be estimated similarly; corrections to the matrix elements due each successive term $|a_{i_1}|^{j_1}\partial_{i_2}^{j-j_1}$ in general are of the order of $v_F(k_F\xi)^{-(j-1)}/l$. Therefore, the linearization procedure in the presence of magnetic field is justified when the condition $(k_F\xi)\gg 1$ is satisfied, and the role of the small parameter is played by both $(k_F\xi)^{-1}$ and $(k_F l)^{-1}\ll 1$, and not only the latter, as is commonly assumed.

Moreover, the "interference" terms relating different nodes ($j\neq j'$) have a similar form and scale as l^{-1}:

$$\left\langle \Psi^{(j)}_{n\mathbf{k}}\middle|\frac{m\mathbf{v}^2}{2}\middle|\Psi^{(j')}_{n'\mathbf{k}'}\right\rangle \propto \frac{v_F}{l}\frac{1}{k_F\xi} \times\left(C_1 e^{i\mathbf{R}_A\cdot\mathbf{G}}+C_2 e^{i\mathbf{R}_B\cdot\mathbf{G}}\right), \quad (22)$$

where $\mathbf{G}=(\mathbf{k}^{(j)}_F+\mathbf{k})-(\mathbf{k}^{(j')}_F+\mathbf{k}')$ and coefficients $C_{1,2}$, determined by the wavefunctions $\chi^{(j\alpha)}_{\mathbf{k},n}$ and $\chi^{(j'\alpha)}_{\mathbf{k}',n'}$ ($\alpha=A,B$), depend on $(n,\mathbf{k};n',\mathbf{k}')$ but not on $\mathbf{k}^{(j)}_F$ or $\mathbf{k}^{(j')}_F$. One therefore generally anticipates that – with $k_F\xi$ kept fixed, as in our model, and other parameters (such as l or μ) freely varied – the spectrum will undergo a complicated evolution, even at the leading order in l^{-1} (c.f. Ref. 19), due to the inter-nodal contribution enhanced by the singular character of wavefunctions near vortices. Note that in the tight-binding lattice model with the nearest neighbor hopping terms only, we are precisely in this situation: in our simplified model, where no self-consistency condition is employed, $k_F\xi$ is a fixed number of order 1 since the role of the cut-off ξ is played by the lattice spacing δ, and k_F is bounded by $(\pi/2)\delta^{-1}$. Even when the self-consistency condition is employed, as long as the uniform system is described by nearest neighbors only, the ratio v_F/v_Δ automatically fixes t/Δ; for a fixed anisotropy of d-wave nodes, $k_F\xi$ is bounded by a number of the order of α_Δ since $v_F/v_\Delta\sim t/\Delta\sim k_F\xi$ and $\xi\sim\delta$, and therefore the simple Simon-Lee scaling limit will be difficult to reach in the strict sense. Of course, one may introduce the next-nearest neighbors and further hopping terms in order to optimize parameters and maximize $k_F\xi$ while retaining the fixed value of α_Δ. In this case, the amplitude of the oscillations will still scale as l^{-1}, albeit with a suitably reduced prefactor.

The above "interference" pattern of the spectrum for a moderately large $(k_F\xi)$ is expected to have a periodic structure, depending on the commensuration of the nodal wavevectors and a magnetic length. Consider a change in chemical potential μ or other parameters that result in a displacement of nodal points at the Fermi surface. If the difference $(\mathbf{k}^{(j)}_F-\mathbf{k}^{(j')}_F)\cdot(\mathbf{R}_B-\mathbf{R}_A)$ changes by a multiple of 2π, then the amplitudes of the matrix elements in (22) between $(n,\mathbf{k})$ and $(n',\mathbf{k}')$, which determine the leading order perturbative corrections to the energy spectrum, are the same to the leading order in l^{-1}, apart from the prefactor $(k_F\xi)^{-1}$. Thus, in addition to overall the Simon-Lee "v_F/l" scaling, the spectrum has periodic oscillations determined by the commensuration of the inter-nodal momentum $\mathbf{k}^{(j)}_F-\mathbf{k}^{(j')}_F$ and the difference $\mathbf{R}_A-\mathbf{R}_B$. More precisely, the spectra for two sets of parameters will be similar whenever the nodal points $(\pm k_D,\pm k_D)$ and $(\pm k_D{}',\pm k_D{}')$ satisfy the condition

$$k_D l - k_D{}' l' = 2\pi n, \quad (23)$$

where n is an integer. This is equivalent to Eq. (19) surmised from the numerical solution.

A remarkable feature of the oscillations seen in Figs. 2 and 3 is that the frequency of oscillations in μ grows rapidly with magnetic field. Incidentally, this suggests a way of incorporating the effect of weak disorder, which is expected to suppress the oscillations, in a relatively simple manner: weak disorder in a full calculation is equivalent to weakly modulated $\mu(\mathbf{r})$. On the other hand, since the spectrum is a rapidly oscillating function of μ, only the quantities averaged over one period of oscillations are of interest. For a typical value of magnetic field ($\sim$ 1 Tesla) the period of oscillations can be estimated to be of order 10 meV. Thus, if a random impurity potential $\mu(\mathbf{r})$ is of comparable magnitude or larger, only the averages of measurable physical quantities over a period of oscillation are observable. In Fig. 5 the density of states (DOS) averaged over the first and the second periods close to half-filling are shown for a variety of magnetic fields. At low energies, DOS is linear in energy and should be associated with the nodal structure of the spectrum *on average*.

We end this section by alerting the reader to the fact that, although we have performed detailed numerical cal-

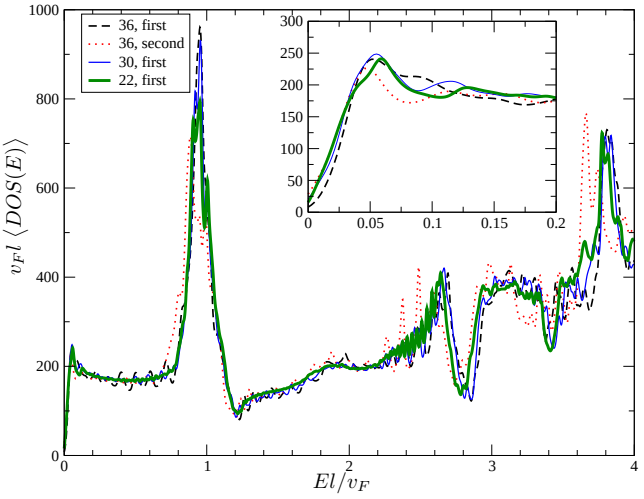


FIG. 5: Full DOS for $\alpha_\Delta = 1$ averaged over one cycle of oscillation in μ for several values of magnetic field characterized by magnetic length l. The density of states was computed for all values of μ on a mesh of size $\delta\mu = 0.02t$ for $l = 22\delta, 30\delta$ and $\delta\mu = 0.01t$ for $l = 36\delta$. The averaged DOS is shown for the first period of oscillations $\mu \in (0, 4t\sin(2\pi\delta/l))$ and for the second period $\mu \in (4t\sin(2\pi\delta/l), 4t\sin(4\pi\delta/l))$. The inset shows the enlarged low-energy part of the figure.

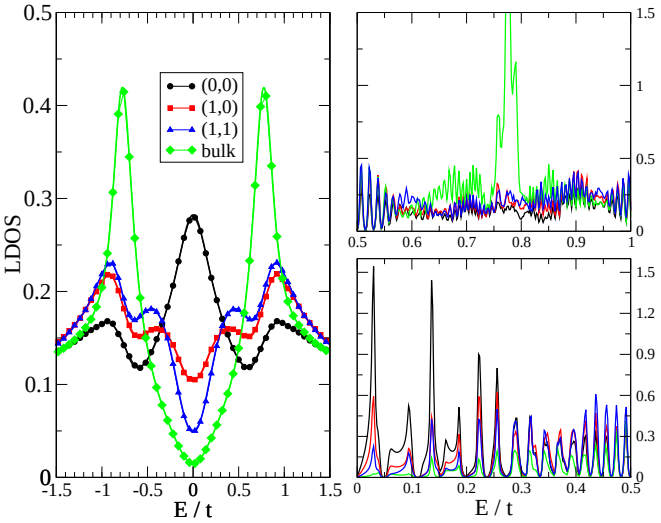


FIG. 6: Left panel: TLDOS at $\mu = 0$ in a mixed state at 4 representative points for $l = 50\delta$ (lines) and $l = 38\delta$ (symbols). Far from the vortices, the TLDOS of a uniform d-wave superconductor is recovered. At four corners of the plaquette containing the vortex the TLDOS exhibits the zero-bias peak[3], while at the next-nearest and the next-next-nearest sites, the TLDOS develops peaks at sub-gap energies. Not only the position of these peaks, but also the thermally broadened TLDOS at all energies does not depend on magnetic field (length) provided that the temperature is larger than a typical width of a band ($T = 0.05t$ here). This large-scale, "high-energy" behavior of the thermally broadened TLDOS should be contrasted with the stark dependence of the low-energy features on l, commensuration effects etc, which we focused on in the previous section. This "fine" structure, which corresponds to true TLDOS is shown on the right, where TLDOS is plotted for $l = 22\delta$. As we described earlier, the latter is generically gapped with the gap scaling as l^{-1} or, as in the example shown in the right panel, is linear for special commensuration between the magnetic length and the Fermi momentum.

culations for the nearest-neighbor hopping model only, where the strict reduction to the simple linearized description is hampered by the enhanced effects of the internodal interference and curvature terms, we expect that in a more elaborate (and more realistic) model, with longer range hoppings, where the condition $k_F\xi \gg 1$ is better satisfied, the linearized effective theory does indeed provide a quantitatively faithful description of the low energy sector of the theory. In that case, the singular nature of the potential due to vortices still requires special care, but such care can be administered by constructing suitable self-adjoint extensions of the linearized Hamiltonian, as belabored in Ref. 21, where a detailed discussion of the Dirac-Bogoliubov-deGennes quasiparticles in singular vortex potentials is presented.

III. TLDOS NEAR VORTICES AND THE MISSING ZERO-BIAS COHERENCE PEAK

So far we were describing the details of the spectrum at the lowest energy scale set by $\hbar v_F/l$. Now we turn to large-scale properties of the TLDOS $g(\mathbf{r}, E)$ – a quantity of direct interest in the STM experiments, which can be expressed through the eigenstates of the BdG Hamiltonian $(u_\mathbf{r}, v_\mathbf{r})$ as

$$g(\mathbf{r}, E) \propto \sum_{n\mathbf{k}} \Big(|u_{n\mathbf{k}}(\mathbf{r})|^2 f'(E - E_{n\mathbf{k}}) + |v_{n\mathbf{k}}(\mathbf{r})|^2 f'(E + E_{n\mathbf{k}}) \Big), \quad (24)$$

where $\mathbf{r}$ denotes the site of the TB lattice and E is the bias. While the results at these large energies are less universal and depend to a much larger degree on the band structure, the spatial profile of the order parameter etc., certain qualitative features turn out to be rather robust and will be discussed in this section.

A typical dependence of the TLDOS on bias for particle-hole symmetric case $\mu = 0$ is shown in Fig. 6 for a set of representative points of the tight-binding lattice. First note that the thermally broadened TLDOS is essentially field-independent once the temperature exceeds the typical width of the field-induced bands, which varies from $C(\alpha_\Delta)\hbar v_F/l$ at low energies, where the spectrum is strongly dispersive to $\hbar\omega_c \sim 2\pi t/l^2$ at energies larger than Δ_c (see Refs. 16,17,19). As an example, compare the TLDOS for $l = 50\delta$ (lines) and $l = 30\delta$ (symbols), which are shown in the left panel of Fig. 6 for temperature $T = 0.05t$.

Far from the vortices the TLDOS is similar to the zero

magnetic field result, and quite naturally the deviations grow progressively stronger as one approaches a vortex. As found by Wang and MacDonald[3], on four cites surrounding the plaquette with the vortex the thermally broadened TLDOS has a pronounced maximum at $E = 0$ as a function of the applied bias voltage, which is called the zero bias conductance peak (ZBCP). Note, however, that ZBCP appears only after thermally broadening the TLDOS, which in its original form is either gapped at general μ or has a linear dependence on the energy for a discrete set of μ such as $\mu = 0$ and $l/\delta = 2 \pmod 4$ as discussed in the previous section (see the right panel of Fig. 6). To resolve this low-energy gapped or linear dependence, however, the temperature must be smaller than a typical width and separation between the bands. We stress that the ZBCP does not correspond to any "localized state": many narrow Bloch bands (see right panel of Fig. 6) merge into a peak after thermal broadening.

Importantly, the situation is very different on the next nearest and next-next nearest neighbor sites around a vortex: there the local density of states exhibits peaks at energies $\approx \pm\Delta_c/2$, where Δ_c denotes the coherence peak energy in a uniform system. Note that these peaks share several similarities with the sub-gap features observed in experiments, namely, the energy of these sub-gap peaks is independent of magnetic field (see left panel in Fig. 6) and it also increases with Δ_c. Again, these peaks do not correspond to any "localized state(s)", as many narrow bands contribute to the peaks after thermal broadening of the LDOS. Although in itself this observation does not quite suffice to explain the absence of ZBCP in experiments, it does suggest that the experimentally observed TLDOS might be reproduced quantitatively by considering a standard d-wave vortex on a lattice with some relatively minor modification, rather than invoking the appearance of additional order parameter(s) within vortex core(s).

A hint of such a minor modification, which could suppresses the ZBCP at the four sites closest to the vortex, comes from a recent analysis of the dopant oxygen atoms in BSCCO. As was noticed by Nunner *et al.*[27], the nature of spatial correlations between the position of the oxygen atoms[28] and features observed in the TLDOS, indicates that the strength of the electron-electron effective pairing coupling constant, and therefore also the magnitude of the d-wave superconducting gap function in BSCCO, are both strongly susceptible to local variations. Variations of Δ by a factor of two or more on a scale of a few lattice spacings, which are basically never seen in conventional superconductors, are routinely observed in BSCCO and other cuprates. In a zero-field case it was found[27] that these modulations of the Δ are likely to be caused by dopant atoms; while the detailed microscopic origin is not clear at this point, it is conceivable that dopant atoms cause local distortions of the atomic lattice and cause spatial variation of the superexchange interaction or other interaction important for superconductivity. Since vortices are expected to be pinned by impurities, the profile of the order parameter near a vortex would consequently differ from that in an ideal model considered so far. Furthermore, even if the vortex is not pinned by an impurity, it may distort the lattice and cause variations of the order parameter near its core that are not described in the canonical BdG scheme, where the pairing interaction constant is assumed to be spatially uniform.

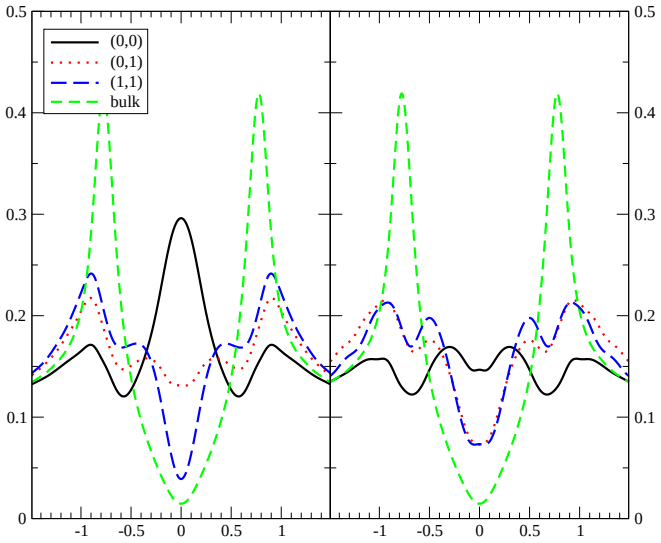


FIG. 7: Left: the thermally broadened TLDOS for a d-wave superconductor with spatially constant amplitude of the gap function, except on four bonds surrounding each vortex, where the gap function is set to zero. The parameters are: $\Delta = 0.2t$, $l = 38\delta$, $\mu = 0$. The temperature is chosen as $T = 0.05t$, and the origin $(0,0)$ denotes the upper-right corner of a plaquette containing the vortex. Note that the nearest sites to the vortex exhibit the ZBCP, while sites $(1,0)$ and $(1,1)$ have sub-gap(sg) peaks at non-zero energies $0.5\Delta_{sg}$. Compared to the case where there is no suppression of $|\Delta_{\mathbf{rr}'}|$ near vortex core, the ZBCP is slightly enhanced. Right: Same, but bond variables on four bonds around each vortex are increased by a factor of 3. Note that this change affects most dramatically the nearest sites $(0,0)$ to the vortex, where the ZBCP is suppressed and two maxima at sub-gap energies develop.

While at this stage the above reasoning in the context of cuprates is only a speculation, it is still a useful phenomenology to examine more closely the effect of such modulation of the d-wave gap function near the vortex core. The main results are summarized in Fig. 7. First, consider a suppression of the gap function all the way to zero on four bonds surrounding plaquette with the vortex; the result is shown in the left panel of Fig. 7. The ZBCP is strongly enhanced, while other features are modified only a little. In the opposite case (see right panel of Fig. 7), when the magnitude of d-wave gap function is locally enhanced, the zero-bias conductance peak is strongly suppressed, the spectral weight is transferred to the $\Delta_c/2$ sub-gap states, and TLDOS acquires a form rather similar to that observed in experiments. The sup-

pression of the ZBCP is even stronger if the bonds with enhanced gap function extend further. Note that in experiments the sub-gap peaks have an energy lower than $\Delta_c/2$: in BSCCO Pan et al. reported[6] the sub-gap(sg) features at $\Delta_{sg} = 7$ meV for the samples with the coherence peak at $\Delta_c = 32$ meV, while Hoogenboom *et al.*[29] cite values $\Delta_{sg} = \pm 14$ meV and $\Delta_c = \pm 45$ meV. In the earliest samples of YBCO, where these low-bias features were observed, Maggio-Aprile *et al.* reported $\Delta_{sg} = \pm 5.5$ meV for system described by $\Delta_c = \pm 20 - 25$ meV. In all cases, the ratio Δ_{sg}/Δ_c ranges from 0.20 to 0.33. Since we used the simplest tight-binding model described by only two parameters (t, μ), the numerical discrepancy between the result $\Delta_{sg}/\Delta_c \approx 0.5$ and the experimentally observed ratios is not unexpected.

Finally, we comment on the 4×4 modulations observed in the vicinity of vortex cores[30,31]. Such modulations are likely to be caused by strong fluctuations of the d-wave order parameter, which are believed to become enhanced near vortices. Explanation of such effects is clearly beyond the scope of the present paper based on a simple mean-field formulation. It has, however, been argued by several groups[32,33,34,35] that even in the absence of magnetic field the enhanced phase fluctuations of the d-wave gap function result in a broken translational symmetry with modulated local average of the gap function. This provides an alternative mechanism of the modulations in the absolute value of Δ.

IV. SINGLE VORTEX PROBLEM

In this section, we study a problem of nodal BdG quasiparticles in presence of a *single vortex* piercing a superconducting grain or droplet of size $L \times L$, where L relates to an external magnetic field in such a way that exactly one superconducting flux $\Phi_0 = hc/(2e)$ fits into the system. A continuum version of a similar problem was considered in Ref. 5, where the delocalized character of the core quasiparticle states was established.

The present problem is technically somewhat easier to handle than the periodic *array* of vortices of the previous sections; however, there are certain general features common to both situations. In particular, the anomalous enhancement of the inter-nodal interference and curvature terms by the $r^{-1/2}$ increase of the wavefunctions near vortex location within the linearized framework still influence the spectrum, albeit now in a less dramatic fashion – unlike the translationally-invariant case considered in previous sections, quasiparticles within an isolated superconducting grain have energy levels that to the leading order in L^{-1} exhibit oscillations as function of $k_D L$ even in the absence of magnetic field. When a magnetic field is turned on, the singularities of the wavefunctions near the vortex result in the halving of the oscillation period.

The starting point for description of the quasiparticles inside such a superconducting grain is still the Hamiltonian (1), except now the BdG wavefunctions $(u(\mathbf{r}), v(\mathbf{r}))$ are required to vanish outside the grain. Alternatively, all bond variables such as $\Delta_{\mathbf{r}\mathbf{r}'}$ or $t_{\mathbf{r}\mathbf{r}'}$ can be set to zero on links along the perimeter of the grain. The remaining bond variables $\Delta_{\mathbf{r}\mathbf{r}'}$ in principle should be determined from the self-consistency conditions, however, just as in the case of the vortex lattice problem, this approach has a drawback of depending on the precise form of the microscopic theory and furthermore on the precise nature of the boundaries. Following our justification from the previous section, and in order to focus on the simplest model with the least number of parameters, we describe the results for the order parameter with a constant amplitude $|\Delta_{\mathbf{r}\mathbf{r}'}|$, its phase simply given by the polar angle around the origin. We verified explicitly that after implementing the self-consistent solution of the problem using the condition (3) we find only small quantitative deviations from the results described in this section, and no change in the qualitative conclusions. Although the "constant amplitude", "polar angle" approximation for the order parameter is violated near the boundaries of the grain, its effect on the physics near the vortex appears insignificant.

Before presenting the numerical results, let us start with several simple observations. Consider again the low-energy effective description of H_{BdG}. The singular gauge transformation and subsequent linearization proceed just as in the case of the vortex lattice problem with the result given by (13), which can be rewritten in the scaling form (14). A significant difference at the level of the linearized description is the presence of external boundary. Although the rescaled Hamiltonian H'_{lin} contains no information on the system size L and the microscopic lengthscale k_F, the spectrum still does not exhibit the scaling

$$E_n = \frac{v_F}{l} F_n(\alpha_\Delta) \ , \tag{25}$$

where F_n is a universal function of the anisotropy α_Δ, as one might initially suspect. Instead, both the boundary conditions at the grain's edge and the singular character of the wavefunctions near the vortex affect the leading order result for the spectrum of the H_{lin}, and consequently violate the simple scaling relation (25), whose more appropriate form should be

$$E_n = \frac{v_F}{l} F_n(\alpha_\Delta, \text{B.C.}) \ . \tag{26}$$

The label B.C. here stands for boundary conditions determined by dimensionless combination $(k_D L)$, that naively might have seemed to drop out of the leading part of the scaling.

As an illustration, consider first a simple example of a zero-field problem – a lattice d-wave superconductor in an empty box with impenetrable walls. The eigenfunctions of the non-linearized problem are given by

$$\psi_{k_x,k_y}(\mathbf{r}) = C \sin(k_x x) \sin(k_y y) \begin{pmatrix} u_{\mathbf{k}} \\ v_{\mathbf{k}} \end{pmatrix} \ . \tag{27}$$

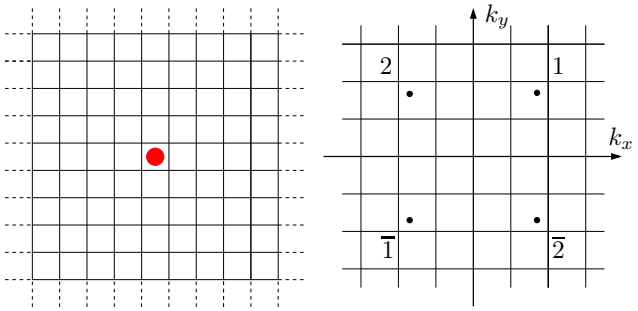


FIG. 8: Left: Superconducting island of size $L \times L$. The tight-binding lattice is shown in black, the red circle is the vortex, and the dashed bonds correspond to the boundary of the superconducting region with both $t_{\mathbf{r}\mathbf{r}'}$ and $\Delta_{\mathbf{r}\mathbf{r}'} = 0$ across the dashed bonds. solid lines. Right: Four nodes of a d-wave superconductor in momentum space at $(\pm k_D, \pm k_D)$, where $k_D = \delta^{-1} \arccos(-\mu/(4t))$, for a general incommensurate case are shown as four circles. The horizontal and vertical lines display the grid of commensurate wavevectors $(\pi n_x/L, \pi n_y/L)$.

where C is a normalization constant, and due to the zero boundary conditions at the edges, we have $k_i = \pi n_i/L$ with positive integer n_x and n_y.

The components of the Nambu spinor $u_{\mathbf{k}}$ and $v_{\mathbf{k}}$ can be expressed as

$$u_{\mathbf{k}}^2 = (1 + \xi_{\mathbf{k}}/E_{\mathbf{k}})/2 \ ,$$
$$v_{\mathbf{k}}^2 = (1 - \xi_{\mathbf{k}}/E_{\mathbf{k}})/2 \ ,$$

where $E_{\mathbf{k}}^2 = \xi_{\mathbf{k}}^2 + \Delta_{\mathbf{k}}^2$. Note that the solution (27) mixes four plane waves $\exp(i\mathbf{k}\cdot\mathbf{r})$ with $\mathbf{k} = (\pm k_x, \pm k_y)$ in a specific combination, and no other combinations are allowed. Among other things, it suggests that simply taking eigenfunctions of the linearized Hamiltonians corresponding to energy E and combining them in all possible combinations in $\psi^{(j)}$ (9) will not work: only special superpositions, which make the full wavefunction vanish at the edges of the system, are allowed. Consider now the lowest energy levels: if the node 1 situated at (k_D, k_D), coincides with one of the allowed mesh points in momentum space $(\pi n_x/L, \pi n_y/L)$, then the lowest energy value is simply zero. Otherwise, depending on anisotropy α_D the lowest energy level is reached at one of the four points of the mesh closest to the node (k_D, k_D). More precisely, if $k_D = \pi n/L + \delta k$ with $|\delta k| < \pi/(2L)$, then the ground state energy is given by the least of $E_{\pi n/L, \pi n/L}$ and $E_{\pi n/L, \pi(n+\mathrm{sgn}(\delta k))/L}$, which to the leading order in $1/L$ equal

$$E_{\pi n/L, \pi n/L} = 4|t \sin(k_D\delta)(\delta k)| \qquad (28)$$

and

$$E_{\pi n/L, \pi(n+1)/L} = 2|\sin(k_D\delta)| \sqrt{t^2 \left(2|\delta k| - \frac{\pi}{L}\right)^2 + \Delta^2 \left(\frac{\pi}{L}\right)^2} \ . \qquad (29)$$

Therefore, the ground state energy is given by (28) when $|\delta k| < (1 + \Delta^2/t^2)\pi/(4L)$, and by (29) otherwise. Note that the result is an oscillating function of k_D changing from zero, whenever $k_D L = \pi n$ and the nodes coincide with mesh points, to

$$2\pi \min(t, \Delta) \sin(k_D\delta)/L = \min(t, \Delta) \frac{2\pi}{L} \sqrt{1 - \frac{\mu^2}{16t^2}} \ .$$

As a result, strictly speaking, there is no uniform scaling (25) of Simon-Lee type even for the zero-field problem, no matter how large the magnetic length L is. Instead, the scaling is fulfilled only on average.

Why do the linearization, and the scaling relation (25) fail? The answer is that in this problem the Fermi momentum scale k_F has not truly been eliminated from the linearized problem. Although the linearized Hamiltonian H'_{lin} does not contain any dependence on k_F, the boundary conditions that should be satisfied by the eigenfunctions of the Hamiltonian *retain* the information on commensuration between k_D and $1/L$. To derive them in general, consider again (9). At the left boundary $x = 0$, and the condition reads

$$e^{ik_D y}\Big(\psi^{(1)}(0,y) + \psi^{(2)}(0,y)\Big) + e^{-ik_D y}\Big(\psi^{(\bar{1})}(0,y) + \psi^{(\bar{2})}(0,y)\Big) = 0 \ . \qquad (30)$$

Since ψ_i vary slowly on the scale of $1/k_F$, we obtain

$$\psi^{(1)}(0,y) + \psi^{(2)}(0,y) = 0 \ , \qquad (31)$$
$$\psi^{(\bar{1})}(0,y) + \psi^{(\bar{2})}(0,y) = 0 \ . \qquad (32)$$

Similarly, the boundary condition at the right edge of the square is

$$e^{ik_D y}\Big(e^{ik_D L}\psi^{(1)}(L,y) + e^{-ik_D L}\psi^{(2)}(L,y)\Big) + e^{-ik_D y}\Big(e^{-ik_D L}\psi^{(\bar{1})}(L,y) + e^{ik_D L}\psi^{(\bar{2})}(L,y)\Big) = 0 \ , \qquad (33)$$

and consequently

$$e^{ik_D L}\psi^{(1)}(L,y) + e^{-ik_D L}\psi^{(2)}(L,y) = 0 \qquad (34)$$
$$e^{-ik_D L}\psi^{(\bar{1})}(L,y) + e^{ik_D L}\psi^{(\bar{2})}(L,y) = 0 \ . \qquad (35)$$

In addition, similar conditions must be satisfied at $y = 0$ and at $y = L$. Note that the conditions on the eigenfunctions of the linearized problem couple different nodes, and moreover they explicitly involve a phase factor $\exp(2ik_D L)$. It is expected, therefore, that the spectrum of the problem does depend on $k_D L$ modulo π even in the leading order of approximation.

The vortex problem adds a new layer of complexity when the linearization is performed. Although in the full, non-linearized problem, the divergence is cut-off at about vortex core radius ξ, and does not pose complications, the effects of the curvature terms such as the inter-nodal

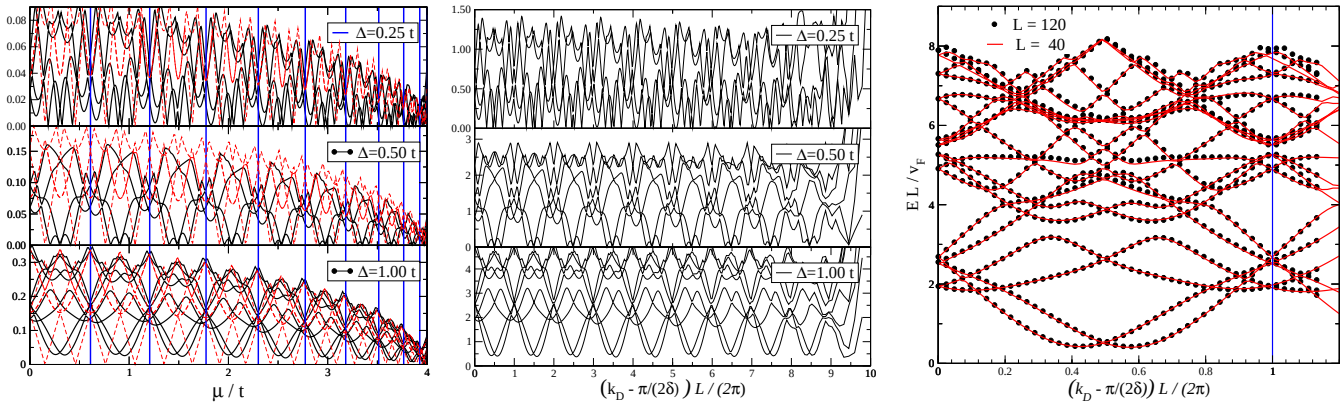


FIG. 9: Left panel: The energy of the lowest 20 energy levels as a function of μ is shown in black solid circles. The three panes of the figure correspond to $\Delta = t/4$, $\Delta = t/2$, and $\Delta = t$. In all cases, the size of the system L equals 41. The red dashed lines are the energies of the lowest four eigenstates of the zero-field problem. Center panel: Rescaled version of the left panel. The rescaled energy $E_n L/(\hbar v_F)$ levels are plotted versus $(k_D - \pi/(2\delta))L/2\pi$. The $\pi/(2\delta)$ offset is artificially introduced to make the plots with different L collapse on the same graph near half filling $\mu = 0$. Right: The energy eigenvalues rescaled as in the center panel are shown for $L = 41\delta$ and $L = 121\delta$. Only the first cycle of the oscillatory pattern is shown for compactness. In both cases, $\Delta = t$.

interference are enhanced due to the singular character of the vortex potential at the linearized Hamiltonian level, as explained in the previous section. A simple estimate similar to (22) shows that as a result, the oscillations of the energy levels are controlled by condition (23), and thereby the periodicity of the energy levels in a grain with a vortex, plotted as a function of $k_D L$, should be doubled compared to the oscillations in an empty grain.

The spectrum of a tight-binding lattice superconductor of size $L \times L$ found numerically in a presence of a single vortex in a magnetic field $HL^2 = hc/(2e)$, is shown in Fig. 9 (left panel). The low-energy quasiparticle spectrum exhibits the following properties: (i) a generic spectrum is gapped, (ii) for $\Delta < \Delta_c$, where $\Delta_c \approx 0.75t$, the zero energy states appear at discrete values of the chemical potential μ, (iii) the spectrum *does not* follow a simple scaling relation (25) displaying instead an oscillatory behavior, with the magnitude of the oscillations scaling as $\hbar v_F/L$, and the period of oscillations decreasing away from $\mu = 0$. The last property is a direct consequence of the approximate 2π-periodicity of the spectrum with respect to $k_D L$: the spectra therefore must be similar at μ and μ' related by $L(k_D(\mu) - k_D(\mu')) = 2\pi n$, where $k_D(\mu) = \arccos(-\mu/(4t)$, and therefore the periodicity condition for $l \gg \delta$, when the equivalent values of μ are closely spaced, can be written as

$$\delta\mu \approx \frac{2\pi}{L}\sqrt{1 - \frac{\mu^2}{16t^2}} \ .$$

Just as in the case of a vortex lattice, it is useful to redisplay the data by extracting the analogue of the overall Simon-Lee scaling factor v_F/L from the energy levels, by plotting EL/v_F vs $k_D L$ (see Fig. 9, center). Clearly, after such rescaling, the dependence of the energy levels on μ (or k_D) is more uniform compared to the raw data plotted in Fig. 9. The oscillatory part of the spectrum, however, also scales as $1/L$ (see Fig. 9, right panel). Note that the periodicity of the oscillations in $k_D L$ is 2π, *twice* the periodicity of the zero-field problem, as expected. The pattern of Fig. 9 holds extremely well for all μ, except near the extreme values close to $\mu \approx -4t$, where the k_F becomes comparable with $1/\delta$, and the linearization procedure is not justified. The commensuration effects could only be experimentally accessible at the temperatures smaller than the amplitude of the oscillations in energy ($\approx \hbar v_F/L$ for the lowest energy levels) The thermally broadened quantities such as the TLDOS will not reflect these oscillations unless the temperature $T \lesssim \hbar v_F/L$. Besides the temperature, impurities, instrumental resolution and other factors could result in broadening the energy levels.

Now we turn to large-energy, short-distance features of the quasiparticle spectrum and describe the TLDOS calculated at temperatures larger than the separation between the energy levels, but still smaller than Δ. This implies sufficiently large L. In practice we used typically $T = 0.05t$ and L ranging from 30δ to 120δ. A representative TLDOS is shown in Fig. 10. The $k_D l$-oscillations at the lowest energy scales $C(\alpha_\Delta)\hbar v_F/L$ are essentially absent in such thermally broadened LDOS. While the resulting TLDOS will still depends on μ (or $k_D l$), the dependence is not oscillatory and merely reflects the slow varying changes of the normal state band structure, yielding large-scale changes such as the position of the van Hove peak. Overall, the spacial and energy distribution of TLDOS is quite similar to the vortex lattice case: the TLDOS at the center of the vortex has a zero-bias coherence peak, while far from a vortex and the edges the TLDOS is similar to the uniform zero-field result, as expected. At the 4 nearest and 4 next nearest neighbors the TLDOS has pronounced peaks at $1/3 - 1/2$ of the

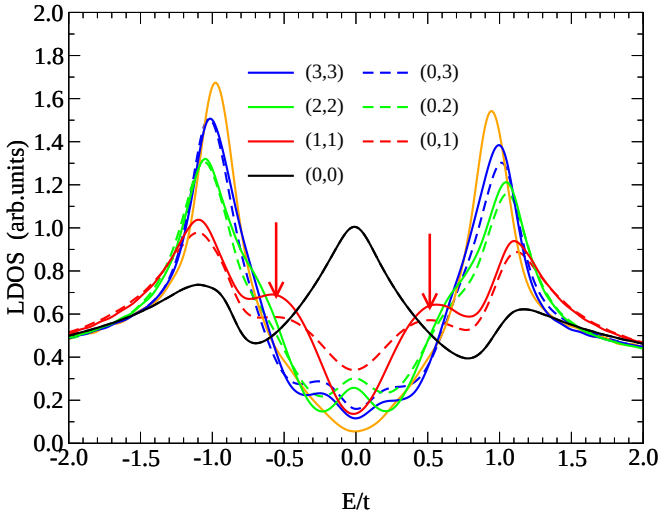


FIG. 10: TLDOS for several sites surrounding the vortex are shown in black, red, green, and blue. The orange line represents TLDOS half-way from the vortex and the boundaries of the system. The black curve with a peak at $E = 0$ represents TLDOS at four sites surrounding the plaquette with the vortex. The parameters used in this figure are $L = 80\delta$, $\mu = 0.2t$, $v_\Delta = 0.25 v_F$; the main structure of the graph is robust under the change of parameters of the model: in particular, at all cites near the vortex, except the four nearest neighbors, the TLDOS has additional peaks at energy $\sim \Delta_c/3 - \Delta_c/2$.

coherence peak energy.

V. CONCLUSIONS

We analyzed the properties of the mixed state in the tight-binding lattice d-wave superconductors by considering a quasiparticle spectrum of i) a vortex lattice and, separately, of ii) an isolated superconducting grain accommodating precisely a single vortex. To reduce the set of free parameters to a manageable number, we restricted ourselves to the simplest tight-binding model, described by only two parameters associated with the normal state (t, μ), and additionally assume that the magnitude of the gap function Δ is spatially uniform. Within a set of simple mean-field microscopic theories, such as those arising from an extended Hubbard or a $t-J$ model, this assumption is well justified since for the parameters suited for to the cuprates, with their short coherence lengths, the self-consistent calculations show that the amplitude of the order parameter recovers its bulk value at distances of only a few lattice spacings.

We find that the low-energy properties of the spectrum are described by Simon-Lee scaling only on *average*, and that both the energy dispersion and the (local) density of states experience oscillations as a function of the chemical potential and a magnetic field. The magnitude of the oscillations in the energy levels behaves as l^{-1} as a function of magnetic length, and therefore it is of the same order as the average Simon-Lee part of the dependence of $E_{n\mathbf{k}}$ on l. We find that in all cases, these oscillations can be well described by a modified Simon-Lee scaling (19), which includes *additional* 2π-periodic dependence of the energy levels on $k_D L$. This modification is shown to be a consequence of the diverging solutions of the "linearized" Hamiltonian. A careful treatment of these divergencies is needed[21], lest one underestimates the quantitative importance of the inter-nodal and formally subleading intra-nodal matrix elements of the Hamiltonian. As a result, the actual expansion parameters of the theory include $k_F\xi$, rather than only $k_F l$, and the scaling of the quasiparticle energy spectrum with respect to magnetic length l is consequently modified.

In addition, we analyzed the large-energy, short-distance features of the quasiparticle spectrum. We found that – apart from the four sites surrounding a vortex where the thermally broadened TLDOS exhibits zero bias conductance peak (ZBCP), in agreement with Refs. 3,5 – the TLDOS on all other sites in the vicinity of a vortex instead show peaks at sub-gap energies. The energy of these sub-gap peaks does not depend on magnetic field, and is determined only by the parameters of the band structure and Δ.

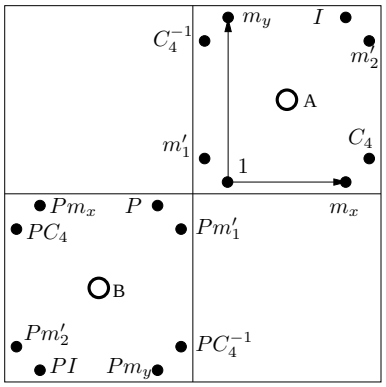
Finally, we examined how the TLDOS is modified when the amplitude of the d-wave gap function is varied locally in the vicinity of the vortex core and found that the suppression of the zero-bias peak corresponds to the enhancement of the d-wave gap function, which could arise through the locally enhanced[27,36] effective pairing interaction constant g. Such enhancement might result from the effect of the impurity atoms pinning the vortices or from a local distortion of atomic lattice by a vortex or fluctuations of d-wave order parameter.

Acknowledgments

We are indebted to O. Vafek for correspondence and stimulating discussions. A.M. would also like to thank B.M. Andersen, A.V. Balatsky, M. Franz, P. J. Hirschfeld, and T. Nunner for discussions. This work was supported in part by the NSF grants DMR-0094981 and DMR-0531159.

APPENDIX: PHASE FACTORS IN THE TIGHT-BINDING HAMILTONIAN

As mentioned in the main text, in principle the bond phase of the order parameter $\theta_{\mathbf{r}\mathbf{r}'}$ should be determined self-consistently. It is convenient, however, to adopt a synthetic approach and approximate $\theta_{\mathbf{r}\mathbf{r}'}$ by using the known solution $\phi(\mathbf{r})$ of the *continuum* Ginzburg-Landau vortex-lattice problem, whose explicit form is given for example in Appendix A of Ref. 21. One may set $\theta_{\mathbf{r}\mathbf{r}'} = \phi[(\mathbf{r}+\mathbf{r}')/2]$ or $\theta_{\mathbf{r}\mathbf{r}'} = (\phi(\mathbf{r})+\phi(\mathbf{r}'))/2$. The latter, which will be predominantly used by us in this article, requires



N	g	$T_g\psi_{\mathbf{r}}$
1	1	$\psi_{g\mathbf{r}}$
2	m_x	$\psi^*_{g\mathbf{r}}$
3	m_y	$\psi^*_{g\mathbf{r}}$
4	m_1'	$\sigma_3\psi^*_{g\mathbf{r}}$
5	C_4	$\sigma_3\psi_{g\mathbf{r}}$
6	m_2'	$\sigma_3\psi^*_{g\mathbf{r}}$
7	I	$\psi_{g\mathbf{r}}$
8	C_4^{-1}	$\sigma_3\psi_{g\mathbf{r}}$

FIG. 11: Left: Point group transformations: equivalent points in the unit cell, which are obtained by action of the group operation g from Table 11 on the reference point 1, are shown as solid circles. Large open circles denote vortices. Right: The symmetry transformations of tight-binding Hamiltonian $\mathcal{H}_{\mathcal{TB}}$. If $\psi_{\mathbf{r}}$ is an eigenstate of energy E, then the states $\psi'_{\mathbf{r}}$ are also eigenfunctions of the Hamiltonian with the same energy, but different momenta in the Brillouin zone listed in the right column of the table. For brevity only a half of all transformations is listed. The remaining half is obtained by applying operator $P\psi_{\mathbf{r}} = \gamma_{\mathbf{r}}\psi_{-\mathbf{r}}$ to each operation in the Table. Thus, overall there are 16 symmetry operations requiring that the spectrum is 16-fold symmetric as shown in the right panel of Fig. 1.

explanation since θ must be defined modulo 2π, while in the form above $\theta_{\mathbf{r}\mathbf{r}'}$ is defined only modulo π. More accurate definition reads

$$\exp(i\theta_{\mathbf{r}\mathbf{r}'}) = \exp\left(i\phi(\mathbf{r}) + \frac{i}{2}\int_{\mathbf{r}}^{\mathbf{r}'} \nabla\phi(\mathbf{r}'')\cdot d\mathbf{r}''\right), \quad \text{(A.1)}$$

where the integral is over the bond connecting $\mathbf{r}$ and $\mathbf{r}'$. It is easy to show that this definition is consistent in the sense that $\exp(i\theta_{\mathbf{r}\mathbf{r}'}) = \exp(i\theta_{\mathbf{r}'\mathbf{r}})$, and provided that $\phi(\mathbf{r})$ does not change by more than π along a bond, the phase $\theta_{\mathbf{r}\mathbf{r}'}$ defined in this way is indeed the "average" of $\phi(\mathbf{r})$ and $\phi(\mathbf{r}')$ in the sense that the "average" is understood as the closest to either $\phi(\mathbf{r})$ (or equivalently $\phi(\mathbf{r}')$) of the two possible choices.

Note that unlike $\theta_{\mathbf{r}\mathbf{r}'}$, phases $\phi^A_{\mathbf{r}}$ and $\phi^B_{\mathbf{r}}$ are not determined by any self-consistent procedure, and merely serve as a technical device to recast the Hamiltonian in a periodic form; we are therefore free to assign their values according to our convenience. Without lost of generality, we choose them by simply evaluating continuous functions $\phi_A(\mathbf{r})$ and $\phi_B(\mathbf{r})$ from the previous section on sites of the tight-binding lattice.

Given definition (A.1), coefficients $\mathcal{V}^A_{\mathbf{r}\mathbf{r}'}$, $\mathcal{V}^B_{\mathbf{r}\mathbf{r}'}$, and $\mathcal{A}_{\mathbf{r}\mathbf{r}'}$ can be easily found from (7) and explicit expressions for $\phi_{A(B)}$ from Appendix A of Ref. 21:

$$e^{i\mathcal{V}^\alpha_{\mathbf{r}\mathbf{r}'}} = e^{i\int_{\mathbf{r}}^{\mathbf{r}'}\mathbf{v}_\alpha(\mathbf{r}'')\cdot d\mathbf{r}''}, \quad \alpha = A, B \quad \text{(A.2)}$$

$$e^{i\mathcal{A}_{\mathbf{r}\mathbf{r}'}} = e^{\frac{i}{2}\int_{\mathbf{r}}^{\mathbf{r}'}(\mathbf{v}_A(\mathbf{r}'')-\mathbf{v}_B(\mathbf{r}''))\cdot d\mathbf{r}''} \quad \text{(A.3)}$$

Since $\mathbf{v}_A(\mathbf{r})$ and $\mathbf{v}_B(\mathbf{r})$ are periodic[19,21], clearly so are $\mathcal{V}^\alpha_{\mathbf{r}\mathbf{r}'}$ and $\mathcal{A}_{\mathbf{r}\mathbf{r}'}$.

The phase factors possess a number of discrete symmetries, which result in the symmetry of the dispersion shown in the right panel of Fig. 1. The full set of the symmetry operations consists of operations g shown in 11 and eight additional transformations Pg, where $P\psi_{\mathbf{r}} \equiv \gamma_{\mathbf{r}}\psi_{-\mathbf{r}}$ is an inversion operator around a midpoint between two (arbitrary) vortices A and B. Each transformation involves a point group operation $g\mathbf{r}$ shown in Fig. 11, which may be followed by complex conjugation and multiplication by Pauli matrix σ_3. Thus, overall there are 16 distinct points in the Brillouin zone with identical set of energy eigenvalues.

Additionally, if $\psi_{\mathbf{r}}$ is an eigenstate of energy E, then $\sigma_2\psi^*_{-\mathbf{r}}$ is an eigenstate of energy $(-E)$ and the same momentum $\mathbf{k}$. Thus, at each point the spectrum is symmetric as a function of energy.

* Electronic address: ashot@phys.ufl.edu
† Electronic address: zbt@pha.jhu.edu

[1] G. E. Volovik, JETP Lett **58**, 469 (1993).
[2] P. I. Soininen, C. Kallin, and A. J. Berlinsky, Phys. Rev. B **50**, 13883 (1994).
[3] Y. Wang and A. H. MacDonald, Phys. Rev. B **52**, R3876 (1995).
[4] Q.-H. Wang, J. H. Han, and D.-H. Lee, Phys. Rev. Lett. **87**, 167004 (2001).
[5] M. Franz and Z. Tešanović, Phys. Rev. Lett. **80**, 4763 (1998).
[6] S. H. Pan, E. W. Hudson, A. K. Gupta, K.-W. Ng, H. Eisaki, S. Uchida, and J. C. Davis, Phys. Rev. Lett. **85**, 1536 (2000).
[7] I. Maggio-Aprile and Ch. Renner and A. Erb and E. Walker and Ø. Fischer, Phys. Rev. Lett. **75**, 2754 (1995).
[8] D. P. Arovas, A. J. Berlinsky, C. Kallin, and S.-C. Zhang, Phys. Rev. Lett. **79**, 2871 (1997).
[9] M. Franz and Z. Tešanović, Phys. Rev. B **63**, 064516 (2001).
[10] J. H. Han and D.-H. Lee, Phys. Rev. Lett. **85**, 1100 (2000).
[11] J. Kishine, P. A. Lee, and X.-G. Wen, Phys. Rev. B **65**, 064526 (2002).
[12] X. Yang and C. Nayak, Phys. Rev. B **65**, 064523 (2002).
[13] C. Wu, T. Xiang, and Z.-B. Su, Phys. Rev. B **62**, 14427 (2000).
[14] P. Nikolic, S. Sachdev, and L. Bartosch, cond-mat/0606001.
[15] S. H. Simon and P. A. Lee, Phys. Rev. Lett. **78**, 1548 (1997).
[16] M. Franz and Z. Tešanović, Phys. Rev. Lett. **84**, 554 (2000).
[17] L. Marinelli, B. I. Halperin, and S. H. Simon, Phys. Rev. B **62**, 3488 (2000).

[18] A. Vishwanath, Phys. Rev. B **66**, 064504 (2002).
[19] O. Vafek, A. Melikyan, M. Franz, and Z. Tešanović, Phys. Rev. B **63**, 134509 (2001).
[20] O. Vafek, A. Melikyan, and Z. Tešanović, Phys. Rev. B **64**, 224508 (2001).
[21] A. Melikyan and Z. Tešanović, cond-mat/0605314.
[22] O. Vafek and A. Melikyan, cond-mat/0509258.
[23] L. P. Gor'kov and J. R. Schrieffer, Phys. Rev. Lett. **80**, 3360 (1998).
[24] P. W. Anderson, cond-mat/9812063.
[25] O. Vafek and Z. Tešanović, cond-mat/0202287.
[26] A. M. is particularly thankful to O. Vafek for discussing this idea.
[27] T. S. Nunner, B. M. Andersen, A. Melikyan, and P. J. Hirschfeld, Phys. Rev. Lett. **95**, 177003 (2005).
[28] K. McElroy, J. Lee, J. A. Slezak, D.-H. Lee, H. Eisaki, S. Uchida, and J. C. Davis, Science **309**, 1048 (2005).
[29] B. W. Hoogenboom and C. Renner and B. Revaz and I. Maggio-Aprile and Ø. Fischer, Physica C **332**, 440 (2000).
[30] J. E. Hoffman, E. W. Hudson, K. M. Lang, V. Madhavan, H. Eisaki, S. Uchida, and J. C. Davis, Science **295**, 466 (2002).
[31] G. Levy, M. Kugler, A. A. Manuel, Ø. Fischer, and M. Li, Phys. Rev. Lett. **95**, 257005 (2005).
[32] H.-D. Chen, O. Vafek, A. Yazdani, and S.-C. Zhang, Phys. Rev. Lett. **93**, 187002 (2004).
[33] Z. Tešanović, Phys. Rev. Lett. **93**, 217004 (2004).
[34] A. Melikyan and Z. Tešanović, Phys. Rev. B **71**, 214511 (2005).
[35] L. Balents, L. Bartosch, A. Burkov, S. Sachdev, and K. Sengupta, Phys. Rev. B **71**, 144508 (2005).
[36] B. M. Andersen, A. Melikyan, T. S. Nunner, and P. J. Hirschfeld, Phys. Rev. Lett. **96**, 097004 (2006).